PHYSICAL REVIEW A **82**, 012501 (2010)

Cross sections for antiproton capture by helium ions

Kazuhiro Sakimoto
Institute of Space and Astronautical Science, Japan Aerospace Exploration Agency, Yoshinodai 3-1-1, Chuo-ku, Sagamihara, Kanagawa 252-5210, Japan

(Received 19 May 2010; published 2 July 2010)

Accurate quantum-mechanical calculations are carried out for antiproton capture by singly ionized He ions, that is, $\bar{p} + \mathrm{He}^+ \rightarrow \bar{p}\mathrm{He}^{2+} + e$, by the combined use of an R-matrix method and direct numerical solution. The total capture cross sections (or collision strengths) and the state distributions of the capture products, $\bar{p}\mathrm{He}^{2+}$, are calculated at collision energies ranging from 0 to 4 eV. The present system is rich in resonances, which appear as a Rydberg series and are characterized as an electron attached to an ion core, $\bar{p}\mathrm{He}^{2+}$. Some resonance levels can be reproduced by a reasonable model based on molecular-quantum-defect theory. The capture into the highest energetically possible state of the products, $\bar{p}\mathrm{He}^{2+}$, always takes place overwhelmingly in the presence or absence of the resonances. However, owing to the resonances, the angular momentum distribution of the products varies considerably depending on the collision energy. The energy-averaged capture cross sections and the capture rate coefficients are also presented for the convenience of future experiments.

DOI: 10.1103/PhysRevA.82.012501 PACS number(s): 36.10.Gv, 32.80.Ee, 34.80.−i

I. INTRODUCTION

Antiproton ($\bar{p}$) capture by atoms or molecules at low collision energies, leading to the formation of antiprotonic atoms, is of fundamental importance as a probe of matter-antimatter interaction [1–3]. The most interesting and simplest capture process is $\bar{p} + \mathrm{H} \rightarrow \bar{p}p + e$. The capture product, $\bar{p}p$, named *antiprotonic hydrogen* (or *protonium*), is a special hydrogenic system made of a particle and its antiparticle. In the $\bar{p} + \mathrm{H}$ system, if the distance between $\bar{p}$ and H is less than the so-called Fermi-Teller critical value $R_{\mathrm{FT}} = 0.639$ a.u., the bound sate of the electron disappears due to the negative charge of $\bar{p}$ [4,5]. For this reason, the $\bar{p} + \mathrm{H}$ system is easily ionizable, and the $\bar{p}$ capture reaction becomes very active in low-energy collisions. The capture process in $\bar{p} + \mathrm{H}$ has not yet been fully understood theoretically although it is the three-body problem [6]. Another interesting $\bar{p}$ capture process as a three-body system is the present subject, that is,

$$\bar{p} + \mathrm{He}^+(1s) \rightarrow \bar{p}\mathrm{He}^{2+}(N,L) + e, \qquad (1)$$

where (N,L) are the principal and angular momentum quantum numbers of the hydrogenic ion $\bar{p}\mathrm{He}^{2+}$. In the case that the target is a singly ionized He ion, the electron is always bound at all the distances between $\bar{p}$ and He^+ in the adiabatic picture based on the Born-Oppenheimer (BO) approximation [7,8], and the *direct* capture probability is found to be very small [9]. However, it is further suggested that the *indirect* (resonance) capture process can be significant owing to the presence of the Coulomb attraction in both the reactant and the product channels [9]. We must properly deal with the resonances to understand the capture mechanism in the $\bar{p} + \mathrm{He}^+$ system.

The resonance states relevant to Eq. (1) must be composed of excited He^+ and rather can be characterized as a collision complex closely correlated with the product channel (i.e., a Rydberg electron attached to an ion core $\bar{p}\mathrm{He}^{2+}$ [10]). If the total energy is less than the separation limit D of $\bar{p} + \mathrm{He}^+$ (i.e., the collision channel $\bar{p} + \mathrm{He}^+$ is closed), the resonance states primarily composed of $\mathrm{He}^+(1s)$ are named *antiprotonic helium*. Some of these resonance states have a very long lifetime ($\gg$1 ps) against (Auger) decay channels and were vigorously investigated in laser spectroscopic experiments [11,12]. The atomic properties of antiprotonic helium measured in the experiments can be compared with elaborate calculations based on the variational method [13–17]. The high-precision study of antiprotonic helium has an important contribution to the determination of fundamental physical constants such as the $\bar{p}$ mass [11,12]. The present study promotes a further understanding of the antiprotonic helium in high-energy states, in addition to gaining an insight into the $\bar{p}$ capture dynamics.

So far, there were various kinds of theoretical approaches to the problem of the $\bar{p}$ capture by atoms and molecules [6]. However, detailed calculations completely based on quantum-mechanical (QM) treatment became realizable only recently. The first effort to perform an accurate QM calculation for $\bar{p} + \mathrm{H}$ was made by the present author [18] by propagating a time-dependent wave packet on grid points in the configuration space. In this sort of direct numerical solution, it is highly desirable that the numerical algorithm is designed using only a single set of coordinates. In Ref. [18], Jacobi coordinates associated with the reactant channel $\bar{p} + \mathrm{H}$ (type I in Fig. 1) were adopted throughout the entire calculation. Because the distance between e and p was explicitly handled as a dynamical variable, their use offered numerical efficiency, especially for the calculation of the electronic motion under the Coulomb attraction. However, the type I coordinates were inappropriate for the asymptotic product channel $\bar{p}p + e$, and hence only the total capture cross sections summed over all the final states were able to be presented in Ref. [18]. If we adopt Jacobi coordinates associated with the product channel $\bar{p}p + e$ (type II in Fig. 1), we can properly describe the state distribution of the products $\bar{p}p$. Instead, we encounter a technical problem: The direct numerical method using the type II coordinates becomes unstable as a solution to the electronic Coulomb motion. This is because the origin of the electron coordinate is the midpoint between p and $\bar{p}$, with the $\bar{p}$ mass being equal to the p mass. Later on, Tong *et al.* [19,20] investigated the state distributions of $\bar{p}p$ in $\bar{p} + \mathrm{H}$ by employing another

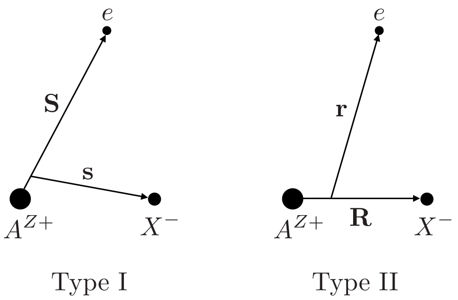

FIG. 1. Two types of Jacobi coordinates. $A^{Z+} = p$ or He^{2+}. $X^- = \mu^-$ or $\bar{p}$.

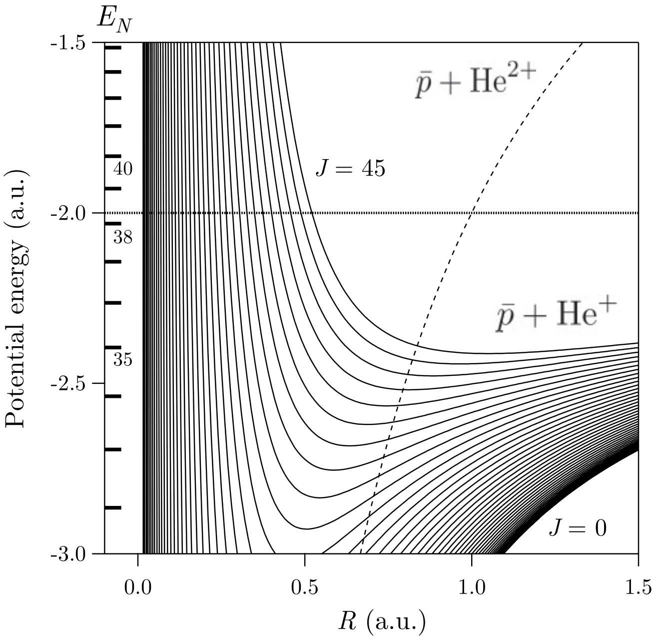

FIG. 2. The sum of the centrifugal and 1σ adiabatic potentials of the $\bar{p} + \mathrm{He}^+$ system as a function of the relative distance R for the total angular momentum quantum numbers $J = 0$–45. Also shown is the Coulomb potential $-2/R$ of the $\bar{p} + \mathrm{He}^{2+}$ system. The $\bar{p}\mathrm{He}^{2+}$ energy levels, E_N, are denoted by horizontal bars on the left side. The energies are measured from that of $\bar{p} + \mathrm{He}^{2+} + e$ at rest. The separation limit of $\bar{p} + \mathrm{He}^+(1s)$ (i.e., the ground-state energy of He^+) is $D = -2$ a.u.

type of time-dependent QM approach and the direct numerical solution. They adopted the type I coordinates as well. In calculating the final-state distributions, they had no choice but to depend on a drastic approximation. Tong *et al.* [21] carried out the calculation of the capture also in the $\bar{p} + \mathrm{He}$ system, by setting the origin of coordinates to the He^{2+} nucleus and further by assuming that the resulting cross term in the kinetic energy operators [22] was negligible. We can expect better numerical efficiency in this coordinate system, which is surely suitable for calculating both the attractive Coulomb motions $e + \mathrm{He}^+$ and $\bar{p} + \mathrm{He}^+$. However, the accuracy of the approximation introduced by Tong *et al.* [21] is quite uncertain. Some other efforts were made to resolve the coordinate problem in the $\bar{p} + \mathrm{H}$ system by using hyperspherical coordinates [23,24]. At the present time, unfortunately, an unphysical approximation was needed for the accomplishment of such numerical calculations.

Recently, careful and rigorous QM studies of the final-state selected capture (or its inverse) process were made for the systems $\bar{p} + \mathrm{He}^+$ [10], $\mu^- + \mathrm{He}^+$ [25], and $\mu^- + \mathrm{H}$ [26,27] by means of a time-independent R-matrix method [28] combined with the direct numerical solution [29]. In these studies, the type II coordinates were adopted, and hence the final-state distribution could be calculated accurately. Because the barycenter of the two heavy particles (A^{Z+} and X^- in Fig. 1) is close to the nucleus, the use of the type II coordinates shows no serious numerical instability in these systems. In reality, the type II coordinates are inappropriate for the asymptotic reactant channel. However, we can circumvent this difficulty by introducing the BO approximation, which is substantially accurate for the description of the reactant channel, especially in the case that the open channel of the target is only the ground $(1s)$ state [9,18]. Therefore, if the nucleus is heavier than the negative particle ($\bar{p}$ or μ^-), there is no need to rely on any questionable approach such as the approximations introduced by Tong *et al.* [19–21].

In this paper, using the R-matrix method of Ref. [29], we report the accurate results of the total and final-state selected cross sections for the capture in the $\bar{p} + \mathrm{He}^+$ system at collision energies E ranging from 0 to 4 eV. The details of the resonance structure are also discussed. The antiprotonic system $\bar{p}\mathrm{He}^{2+}$ produced in the capture cannot permanently survive because of the strong (hadron) interaction [3]. Experimental studies can be found for $\bar{p}\mathrm{He}^{2+}$ [3,30,31], and these provided the valuable information about the strong interaction. In the present study, however all the particles, e, $\bar{p}$, and He^{2+}, are assumed to be point charges and the spin is neglected. (The effect of the strong interaction on the capture process is briefly discussed in Sec. IV.) In Fig. 2, we show the $\bar{p}\mathrm{He}^{2+}$ energy levels E_N and the effective potentials of the $\bar{p} + \mathrm{He}^+$ system, that is, the sum of the centrifugal potential and the lowest (1σ) adiabatic potential. The ground-state energy of $\bar{p}\mathrm{He}^{2+}$ is $E_{N=1} \simeq -80$ keV. All the capture channels that have $N \leqslant 38$ are energetically open even in the limit as $E \to 0$: The reaction is enormously exoergic. The channel $N = 39$ becomes additionally open when the collision energy is $E > E_{N=39} - D = 1.936$ eV. In the present energy range ($E \leqslant 4$ eV), the channels $N \geqslant 40$ are closed ($E_{N=40} - D = 4.527$ eV). Thus, very high states of $N \lesssim 40$ are necessarily involved in the present $\bar{p}$ capture process. Accordingly, we must carry out the collision calculations for the total angular momentum quantum numbers $J \lesssim 40$. Owing to the Coulomb attraction between $\bar{p}$ and He^+, this remains true even at $E \to 0$. In the previous R-matrix study for the $\bar{p} + \mathrm{He}^+$ system [10], only a limited range of J was taken into account. To obtain the capture cross sections, here we perform the R-matrix calculations for $J = 0$–40.

II. THEORY AND CALCULATION

The detailed description of the theoretical formulation and the numerical method for the collision system of a heavy negative particle and a He^+ ion can be found elsewhere [10,25,29] and is not repeated here. Only a brief summary is given. We use atomic units (a.u.) unless otherwise stated.

We consider the three-body system of $\bar{p}$, He^{2+}, and e. We adopt the Jacobi coordinates $(\mathbf{R},\mathbf{r})$ associated with the product channel $\bar{p}$He$^{2+}+e$ (type II in Fig. 1): $\mathbf{R}$ is the position vector of $\bar{p}$ from He^{2+}, and $\mathbf{r}$ is that of e from $\bar{p}$He^{2+}. The time-independent Schrödinger equation for the collision problem is

$$\mathcal{H}\Psi^{JM}(\mathbf{R},\mathbf{r}) = E_{\text{tot}}\Psi^{JM}(\mathbf{R},\mathbf{r}), \tag{2}$$

where (J,M) are the total angular momentum quantum numbers and E_{tot} is the total energy, which is higher than the separation limit ($D=-2$ a.u.) of $\bar{p}+\text{He}^{+}(1s)$ in the present study. The Hamiltonian $\mathcal{H}$ is given by

$$\mathcal{H} = -\frac{1}{2m_R}\frac{\partial^2}{\partial\mathbf{R}^2} - \frac{1}{2m_r}\frac{\partial^2}{\partial\mathbf{r}^2} + V, \tag{3}$$

with the Coulomb interactions

$$V = -\frac{2}{R} - \frac{2}{|(m_R/m_\alpha)\mathbf{R}+\mathbf{r}|} + \frac{1}{|(m_R/m_{\bar{p}})\mathbf{R}-\mathbf{r}|} \tag{4}$$

and the reduced masses

$$m_R = \frac{m_{\bar{p}}m_\alpha}{m_{\bar{p}}+m_\alpha}, \quad m_r = \frac{m_e(m_{\bar{p}}+m_\alpha)}{m_e+m_{\bar{p}}+m_\alpha}, \tag{5}$$

where m_e (=1 a.u.) is the e mass, $m_{\bar{p}}$ is the $\bar{p}$ mass, and m_α is the He^{2+} (α particle) mass.

In the type II coordinates, the product (electron emission and capture) channel $\bar{p}$He$^{2+}+e$ is rigorously defined by the electronic angular momentum quantum number l and the principal and angular momentum quantum numbers (N,L) of the hydrogenic system $\bar{p}$He^{2+} with the energy

$$E_N = -\frac{2m_R}{N^2}. \tag{6}$$

In the product region, the wave function $\Psi^{JM}(\mathbf{R},\mathbf{r})$ can be given by

$$\Psi^{JM}(\mathbf{R},\mathbf{r}) = (Rr)^{-1}\sum_{NLl}\mathcal{Y}^{JM}_{Ll}(\hat{\mathbf{R}},\hat{\mathbf{r}})\Upsilon_{NL}(R)f^{J}_{NLl}(r), \tag{7}$$

where $\mathcal{Y}^{JM}_{Ll}(\hat{\mathbf{R}},\hat{\mathbf{r}})$ is the eigenfunction of the total angular momentum, and $\Upsilon_{NL}(R)$ is the radial Coulomb function of $\bar{p}$He^{2+}. For the reactant channel $\bar{p}+\text{He}^{+}$, we assume the lowest adiabatic state (1σ). In this case, it is sufficient to consider only the total parity of $(-1)^{L+l}=(-1)^{J}$, which is not shown explicitly in the present formulation. In the reactant region, the wave function $\Psi^{JM}(\mathbf{R},\mathbf{r})$ can be written as

$$\Psi^{JM}(\mathbf{R},\mathbf{r}) = (Rr)^{-1}\mathcal{D}^{J}_{M0}(\hat{\mathbf{R}})\chi_{1\sigma}(R;r,\theta)F^{J}_{1\sigma}(R), \tag{8}$$

where $\chi_{1\sigma}(R;r,\theta)$ is the wave function of the 1σ adiabatic state, θ is the angle between $\mathbf{R}$ and $\mathbf{r}$, and

$$\mathcal{D}^{J}_{M\lambda}(\hat{\mathbf{R}}) = \left[\frac{2J+1}{16\pi^2(1+\delta_{\lambda,0})}\right]^{1/2} \times \left[D^{J}_{M\lambda}(\hat{\mathbf{R}}) + (-1)^{\lambda}D^{J}_{M,-\lambda}(\hat{\mathbf{R}})\right]^{*} \tag{9}$$

is the symmetrized and normalized form of the Wigner D function $D^{J}_{M\lambda}(\hat{\mathbf{R}})$.

We employ the R-matrix method for the solution to the collision problem [29]. In the inner region defined by $0\leqslant R\leqslant A$ and $0\leqslant r\leqslant a$, we consider the R-matrix eigenvalue equation:

$$[\mathcal{H}+\mathcal{L}]\Phi^{JM}_{\rho}(\mathbf{R},\mathbf{r}) = E^{J}_{\rho}\Phi^{JM}_{\rho}(\mathbf{R},\mathbf{r}), \tag{10}$$

where

$$\mathcal{L} = \frac{1}{2m_RA}\delta(R-A)\frac{\partial}{\partial R}R + \frac{1}{2m_ra}\delta(r-a)\frac{\partial}{\partial r}r \tag{11}$$

is the Bloch operator [32], and ρ identifies the discrete eigenvalues E^{J}_{ρ}. In the numerical calculation, the wave function Φ^{JM}_{ρ} is expanded in the form

$$\Phi^{JM}_{\rho}(\mathbf{R},\mathbf{r}) = (Rr)^{-1}\sum_{\lambda\geqslant 0}\mathcal{D}^{J}_{M\lambda}(\hat{\mathbf{R}})\phi^{J\lambda}_{\rho}(R,r,\theta), \tag{12}$$

where λ is the electronic magnetic quantum number around $\hat{\mathbf{R}}$. Then, we solve $\phi^{J\lambda}_{\rho}(R,r,\theta)$ numerically, and we can obtain the R matrix by projecting the wave function Φ^{JM}_{ρ} onto the channel functions $\mathcal{Y}^{JM}_{Ll}(\hat{\mathbf{R}},\hat{\mathbf{r}})\Upsilon_{NL}(R)/R$ and $\mathcal{D}^{J}_{M0}(\hat{\mathbf{R}})\chi_{1\sigma}(A;r,\theta)/r$ at the boundary.

From the R-matrix elements, we can calculate the scattering S matrix elements $(\mathbb{S}^{J})_{NLl,1\sigma}$ for the $\bar{p}$ capture [29]. The probability of the capture into the (N,L,l) product channel is

$$P^{J}(N,L,l) = |(\mathbb{S}^{J})_{NLl,1\sigma}|^2. \tag{13}$$

We define the total capture probability summed over all these channels by

$$P^{J} = \sum_{NLl}P^{J}(N,L,l). \tag{14}$$

Introducing the total collision strength Ω defined by

$$\Omega = \sum_{J}(2J+1)P^{J}, \tag{15}$$

which is a useful quantity when we discuss low-energy collisions in the Coulomb system [9,33], we can give the total capture cross section in the form

$$\sigma = \frac{\pi\Omega}{2mE}, \tag{16}$$

where the reduced mass $m=m_{\bar{p}}(m_\alpha+m_e)/(m_{\bar{p}}+m_\alpha+m_e)$ is virtually equal to m_R, and $E=E_{\text{tot}}-D$ is the collision energy of $\bar{p}+\text{He}^{+}$. For the final-state selected capture collision strengths, we can introduce

$$\Omega(N,L) = \sum_{Jl}(2J+1)P^{J}(N,L,l) \tag{17}$$

and

$$\Omega(N) = \sum_{L}\Omega(N,L), \quad \Omega(L) = \sum_{N}\Omega(N,L). \tag{18}$$

Using these quantities, we can give the final-state selected capture cross sections in the same way as Eq. (16). The energy distribution of the emitted electrons may be defined by

$$f(\varepsilon) = \frac{1}{\sigma}\frac{d\sigma}{d\varepsilon} = \frac{N^3\Omega(N)}{4m_R\Omega}, \tag{19}$$

where $\varepsilon = E_{\text{tot}}-E_N$ is the electron kinetic energy.

The wave function $\phi_\rho^{J\lambda}(R,r,\theta)$ in Eq. (12) was calculated directly on the grid points in the (R,r,θ) coordinate space [29]. As in Ref. [10], we took the boundary values $A = 1.3$ a.u. and $a = 3.5$ a.u. and the numbers of grid points $(N_r,N_\theta) = (30,5)$ in the (r,θ) coordinates. The number of gird points in the R coordinate was chosen differently ($N_R = 50$–200) according to J. We considered the channels of $\lambda \leqslant 1$ and $l \leqslant 3$. We needed to further propagate the R matrix from $r = a$ to a large distance $r = 50$ a.u. to eliminate long-range coupling effects [10,29].

III. RESULTS AND DISCUSSION

A. Resonances

In the case of $E_{\text{tot}} \sim -3$ a.u. $< D$ (i.e., $E < 0$), the resonance states (antiprotonic helium) can be identified as the vibrational motion supported by the 1σ adiabatic potential [8,11]. For the resonances relevant to the capture process (i.e., $E > 0$), however, such an adiabatic picture is no longer appropriate. Instead, we can introduce an idea that the resonance state is composed of an ion core $\bar{p}\text{He}^{2+}$ and an outer electron (a Rydberg picture) [10]. Also in the $\mu^- + \text{He}^+$ system, the Rydberg picture was found to be useful for a systematic study of the resonances relevant to the μ^- capture process [25].

In Fig. 3, we present the total capture probabilities P^J for all the J that contribute to the cross sections at collision energies $0 \leqslant E \leqslant 1.85$ eV. We can see a lot of resonances for any J. To roughly examine the properties of these resonances, first we consider a simplified version of the Rydberg picture (a hydrogenic model), in which the core $\bar{p}\text{He}^{2+}$ is assumed to be a point charge and the resonance energy is expressed as

$$E^{\text{H}}_{N_c n} = E_{N_c} - \frac{1}{2n^2}, \qquad (20)$$

where $N = N_c$ indicates the closed channel in $e + \bar{p}\text{He}^{2+}$, and n is the principal quantum number of the electron. The series limit ($n \to \infty$) of the resonances is the excited-state energy E_{N_c} of $\bar{p}\text{He}^{2+}$. In the range of the collision energies E shown in Fig. 3, the most important closed channel is $N_c = 39$, which has the threshold $E_{N_c=39} - D = 1.936$ eV. We can see that the present resonances satisfy the requirements for the justification of the Rydberg picture: The size of the ion core [$\sim N_c^2/(2m_R) \simeq 0.5$ a.u.] is much smaller than the average radius of the electron orbit ($\sim n^2$ for $n \geqslant 2$). Figure 3 shows that most of the resonances can be basically identified as the hydrogenic states $n \geqslant 3$ associated with $N_c = 39$. Another hydrogenic $(N_c,n) = (40,2)$ level is present at $E = 1.126$ eV near the $(N_c,n) = (39,3)$ level ($E = 1.085$ eV). It is certainly possible that these two adjacent levels are strongly coupled with each other. Indeed, as discussed later, some complicated J-dependent behavior of the resonances at $E \simeq 1$ eV can be attributable to this coupling effect.

We can see that the probability of the off-resonance (i.e., direct) capture is always very small ($\lesssim 0.03$). If the resonances were absent, the $\bar{p}$ capture would not be a notable reaction channel in the $\bar{p} + \text{He}^+$ system. Actually, a resonance can yield a large capture probability (occasionally close to unity), and there are plenty of such resonances. It is evident that the resonance plays a very important role in the $\bar{p}$ capture by He^+, as was suggested in Ref. [9].

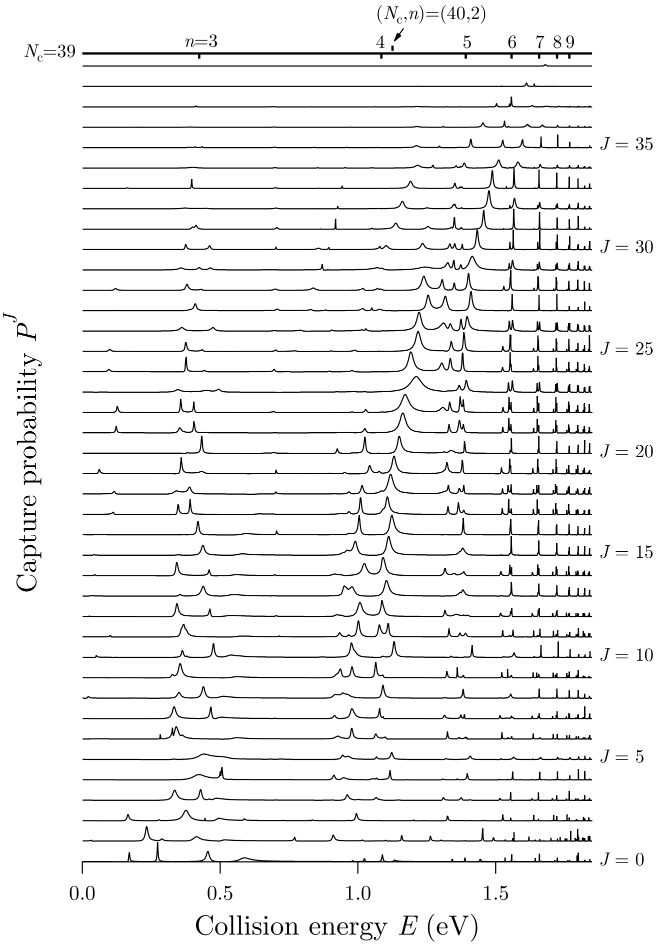

FIG. 3. The total capture probabilities P^J for the total angular momenta $J = 0$–39 at collision energies $0 \leqslant E \leqslant 1.85$ eV. The hydrogenic levels $E^{\text{H}}_{N_c n} - D$ for $N_c = 39$ and 40 are denoted by vertical bars on the top of the figure.

B. Quantum-defect-theory model

The ion core $\bar{p}\text{He}^{2+}$ of the resonance complex is the hydrogenic Coulomb system and also the two-body heavy-particle system. As seen in Sec. III A, this core is always in a very high N state, and hence it has a long period of internal motion. In such a case, we may regard the core $\bar{p}\text{He}^{2+}$ as a kind of molecule (i.e., a diatomic molecule with a vibrational quantum number $v = N - L - 1$ and a rotational quantum number L). Thus, the present resonance state is similar to a molecular Rydberg state, and we can expect that molecular quantum defect theory (QDT) [33,34] is applicable to the analysis of the resonances. By using QDT, the scattering K matrix elements associated with the closed channels can be given by [34]

$$(\mathbb{K}^J)_{N_c'L'l',N_cLl} = \sum_{\lambda} U^{Jl}_{L'\lambda}\langle\Upsilon_{N_c'L'}|\tan[\pi\eta_{l\lambda}(R)]|\Upsilon_{N_cL}\rangle\, U^{Jl}_{L\lambda}\,\delta_{ll'}, \qquad (21)$$

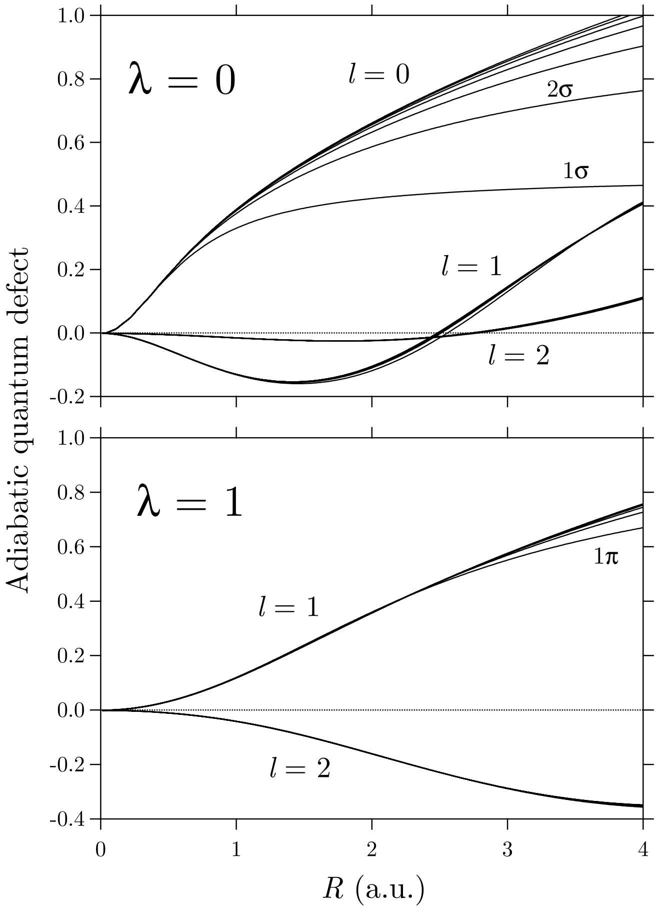

FIG. 4. Adiabatic quantum defects $\eta_{l\lambda}(R)$ for various BO states as a function of the relative distance R.

where $\eta_{l\lambda}(R)$ is the R-dependent adiabatic quantum defect obtained in the BO approximation, and $U^{Jl}_{L\lambda}$ is the matrix elements of the transformation between the molecular and space-fixed frames [34]. The adiabatic quantum defects $\eta_{l\lambda}(R)$ are assumed to be identified by the quantum numbers (l,λ), and these are shown in Fig. 4. (Strictly speaking, the suffix l in $\eta_{l\lambda}(R)$ is not coincident with the electronic angular momentum defined in Sec. II.) We can see that the quantum defects (except for the ground adiabatic state 1σ) belonging to the same label (l,λ) are well approximated by a single curve in the important range ($R \lesssim 1$ a.u.) of the integration in Eq. (21) (cf. Fig. 2). If the coupling between the resonance and continuum states is weak, the resonance energy may be given by the condition [33]

$$\det[\tan(\pi\nu) + \mathbb{K}^J] = 0, \tag{22}$$

where ν is the effective quantum number defined by

$$E_{\mathrm{tot}} = E_{N_{\mathrm{c}}} - \frac{1}{2\nu^2}. \tag{23}$$

For the energies $E < 1.936$ eV, the closed channels of $N_{\mathrm{c}} = 39$ and 40 were included in the calculation of Eq. (22).

For several total angular momenta J, we show in Fig. 5 the total capture probabilities P^J at energies $0 \leqslant E \leqslant 1.6$ eV in detail and also the energy levels obtained by the QDT method for the s, p ($n = 3$–6) and d ($n = 3$) Rydberg electrons and the $N_{\mathrm{c}} = 39$ and 40 cores. For $J = 5$ (and probably also $J = 15$), almost all the resonance positions can be identified as the QDT levels associated with only $N_{\mathrm{c}} = 39$. The QDT method seems to work nicely for low J. However, as J increases, there appear several resonance levels (labeled X and Y), which cannot be identified by the present QDT model. Of these, the resonance (Y) at $E \simeq 1.2$ eV for $J = 25$ has a noticeably large probability and contributes importantly to the capture. In the case of $J = 25$, we can find that each of the two QDT levels associated with $N_{\mathrm{c}} = 40$ is very close to a QDT level associated with $N_{\mathrm{c}} = 39$. The former levels are recognized as the p Rydberg state while the latter are as the s state. Because l is assumed to be conserved in Eq. (22), the coupling between these adjacent levels cannot be taken into account in the present QDT model. Actually, the $e + \bar{p}\mathrm{He}^+$ system has an anisotropic interaction, and hence the l mixing would not be negligible.

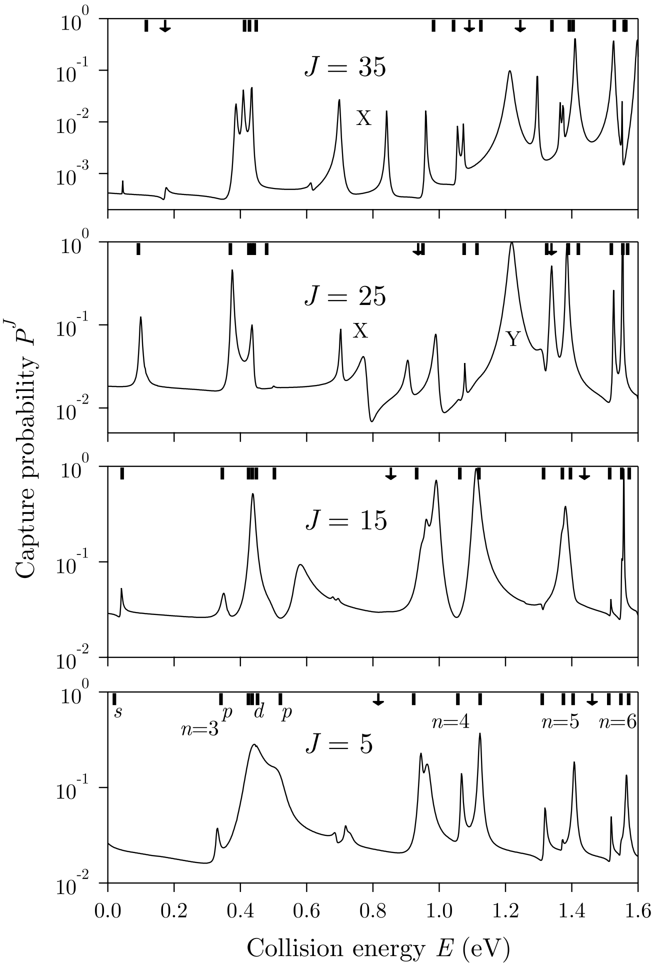

FIG. 5. The total capture probabilities P^J for the total angular momenta $J = 5, 15, 25,$ and 35 at collision energies $0 \leqslant E \leqslant 1.6$ eV. The energy levels obtained by the QDT method are denoted by vertical bars ($N_{\mathrm{c}} = 39$) and vertical arrows ($N_{\mathrm{c}} = 40$) on the top of each panel.

It is conceivable that the resonance can have an important contribution to the capture process if the resonance state consists mainly of the s or p Rydberg electron. Figure 6 shows the energy levels in the range $0 \leqslant E \leqslant 1.85$ eV obtained by using the QDT model for the s and p Rydberg electrons; it is directly comparable to Fig. 3 for all the total angular

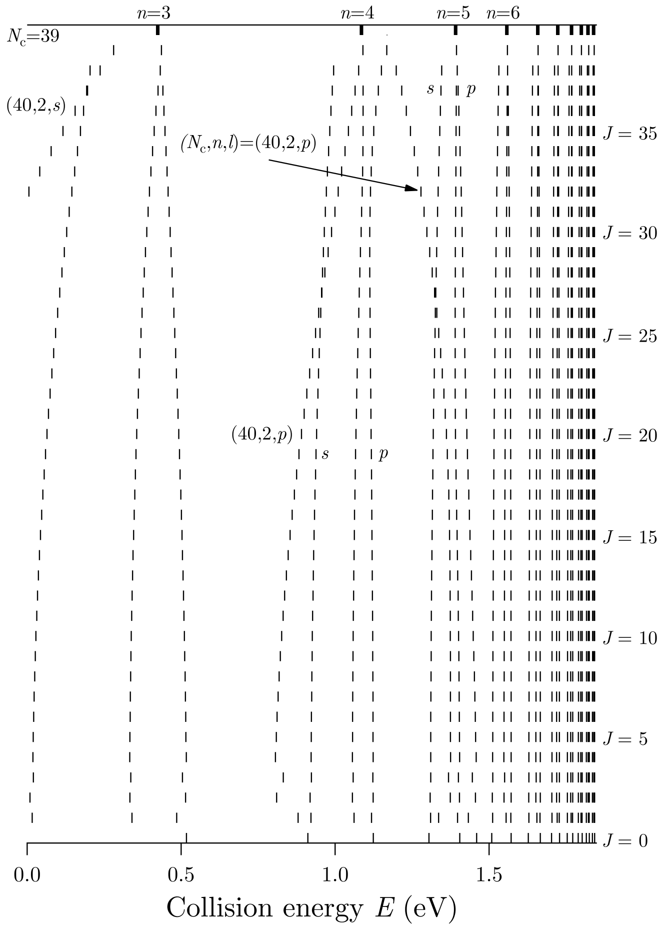

FIG. 6. An energy level diagram obtained by the QDT method for the s and p Rydberg electrons. The results are shown for the total angular momenta $J = 0$–39 in the range of collision energies $0 \leqslant E \leqslant 1.85$ eV (cf. Fig. 3). The hydrogenic levels $E^{\mathrm{H}}_{N_c=39,n} - D$ are denoted by vertical bars on the top of the figure.

momenta J. Figure 6 may be helpful for our understanding the major J dependence of the resonance energy levels. As J increases, the QDT levels seem to converge with the hydrogenic one ($E^{\mathrm{H}}_{N_c n} - D$). If the core is a point charge, there exits a degeneracy of the hydrogenic levels with the same (N_c,n). The splitting of the degenerate levels occurs according to the core effect. This indicates that the core effect becomes more significant for lower J. As was discussed in Ref. [25], the importance of the core effect can be explained in terms of the overlap among the core wave functions $\Upsilon_{N_c L}$: If J is low (i.e., L is low, considering $L \sim J$), we have a large overlap among $\Upsilon_{N_c L}$ for a fixed N_c [25] and hence the large matrix elements $(\mathbb{K}^J)_{N_c L' l, N_c L l}$ resulting from Eq. (21) produces a large level shift. The partial wave $J = 39$ has a special situation for the resonances associated with $N_c = 39$: Only a single level appears for each n because the angular momentum $L = J$ or $J + 1$ ($\geqslant N_c = 39$) is forbidden.

In Fig. 6, we can see that the splitting behavior of the (N_c,n) = (40,2) levels as a function of J is largely different from those of the other $N_c = 39$ levels. As a result, the level energy versus J exhibits a structure like curve crossing, for example, near the points of ($E = 0.196$ eV, $J = 37$), ($E = 0.957$ eV, $J = 27$), and ($E = 1.323$ eV, $J = 27$). Of particular importance are the latter two crossing points, at which the (N_c,n,l) = (40,2,p) levels cross with the (N_c,n,l) = (39,4,s) and (39,5,s) levels. These crossings can actually occur because, as mentioned previously, the l mixing is not taken into account in Eq. (22). Near these crossing points, however, the s-p coupling should be very important. The neglect of the l mixing is expected to be the main reason that the present QDT model cannot explain several resonances (X and Y) in the energy range $0.7 \lesssim E \lesssim 1.2$ eV for $J = 25$ and 35 shown in Fig. 5.

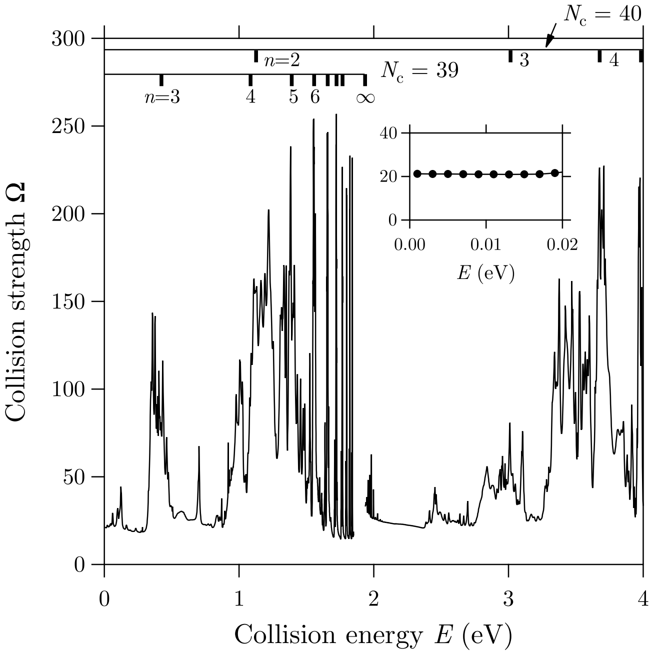

FIG. 7. The capture collision strengths Ω summed over all the final product channels at collision energies $0 \leqslant E \leqslant 4$ eV except for those just below the $N = 39$ channel threshold. The hydrogenic levels $E^{\mathrm{H}}_{N_c,n} - D$ for $N_c = 39$ and 40 are denoted by vertical bars on the top of the figure. Inserted is the enlarged figure of the capture collision strengths Ω at collision energies $0 \leqslant E \leqslant 0.02$ eV.

C. Capture collision strength

We calculated the capture collision strengths Ω at energies $E \leqslant 4$ eV, and the results are shown as a function of E in Fig. 7. As can be seen in Fig. 3 or 6, the resonance position shifts with a change in J, and the extent of its shift is not always negligibly small compared with the resonance width. For this reason, summing over all the related partial waves J yields a highly complicated resonance structure in the collision strength. Nevertheless, we can still recognize a Rydberg series of resonances converging to the $N = 39$ channel threshold $E_{N=39} - D$. (The resonances become too dense at energies just below $E_{N=39} - D$, and hence no data are presented there in the figure.) In the μ^- capture by He$^+$ [25], a cluster of resonances belonging to the same (N_c,n) can be apparently split into two groups, and it appears in the form of bimodal major peaks. However, no such structure can be observed clearly in the present case. There is a jump in the collision strength at $E = E_{N=39} - D$ due to the threshold effect in the Coulomb system $\bar{p}\mathrm{He}^{2+} + e$ [33,35].

The Coulomb attraction works also in the reactant channel $\bar{p} + \mathrm{He}^+$, and the capture reaction is exoergic. For this reason, in the limit as $E \to 0$, the collision strength remains finite, and the capture cross section diverges as E^{-1} [9]. At the lowest energy $E = 0.001$ eV considered here, we have $\Omega = 21.2$. If the collision strength is assumed to be constant at $E < 0.001$ eV (as can be expected in Fig. 7), then the low-energy behavior of the capture cross section is estimated to be

$$\sigma \text{ (in a.u.)} = \frac{C}{E \text{ (in eV)}} \quad \text{for } E \leqslant 0.001 \text{ eV}, \tag{24}$$

where $C = 0.618$. The nonzero and constant nature of the collision strength at low energies are well known in electron scattering from ions [33]. For a negative particle X^-, if m' denotes the reduced mass of $X^- + \mathrm{He}^+$, the partial waves of the angular momentum J up to $J_0 = (m')^{1/2} - 1$ can participate in the capture at $E \sim 0$ ($J_0 \simeq 37$ for $X^- = \bar{p}$) [9]. Assuming $P^J = 1$ and summing it over $0 \leqslant J \leqslant J_0$ in Eq. (15), as the upper bound of the capture cross section at energies $E \sim 0$, we have $\sigma_{\mathrm{upper}} = \pi/(2E)$, which is independent of m'. In the form of Eq. (24), this gives $C_{\mathrm{upper}} = 42.7$. In the adiabatic picture, the X^- capture reaction is treated as a nonadiabatic process. If the resonance is absent, there is no reason for the nonadiabatic coupling to become important in the $X^- + \mathrm{He}^+$ system. This presents in the way of $C \ll C_{\mathrm{upper}}$. For the μ^- capture by He^+, the value of C was determined to be $C_{\mu^-} = 3.33$ [25], which is larger than the value for the $\bar{p}$ capture. As a matter of course, the nonadiabatic coupling should be stronger for a lighter X^- mass. (The $\bar{p}$ mass is about nine times heavier than the μ^- mass.) The situation is quite different from that in the $X^- + \mathrm{H}$ system. Irrespective of the X^- mass, the capture cross sections for the neutral target are very close to the Langevin value, which can be regarded as the upper bound at low energies [27,36].

Figure 8 shows the capture collision strengths $\Omega(N)$ for the formation of $\bar{p}\mathrm{He}^{2+}(N)$ with the principal quantum number N specified. At collision energies $E \leqslant 1.8$ eV (below the $N = 39$ threshold), the collision strength $\Omega(N)$ at the same energy becomes the largest always for $N = 38$, which is the highest open capture channel. If $1.95 \leqslant E \leqslant 4$ eV (above the $N = 39$ threshold), then the most populated state becomes $N = 39$, which is the highest one at these energies. The upper panel of Fig. 9 shows the N distribution $\Omega(N)/\Omega$ of the products $\bar{p}\mathrm{He}^{2+}$ at three collision energies above the $N = 39$ threshold. Regardless of whether resonances are present, the N distributions are nearly a monotonically decreasing function of N, and the capture into the highest energetically possible state occurs overwhelmingly. As a result, the average principal quantum number $\langle N \rangle$ is always very close to the highest possible value 39 (or 38) (Fig. 10). The kinetic energy distribution $f(\varepsilon)$ of the emitted electrons is plotted in the lower panel of Fig. 9. Because the highest open channel N has the largest population, the capture mainly leads to the emission of slow electrons, as was found also in the $\mu^- + \mathrm{He}^+$ system [25]. At the collision energy $E = 2$ eV, which is just above the $N = 39$ threshold (1.936 eV), a lot of electrons are emitted with only a small kinetic energy $\varepsilon = 0.064$ eV. The capture into very low N states is practically forbidden because the emission of electrons having extremely high energies is unrealistic.

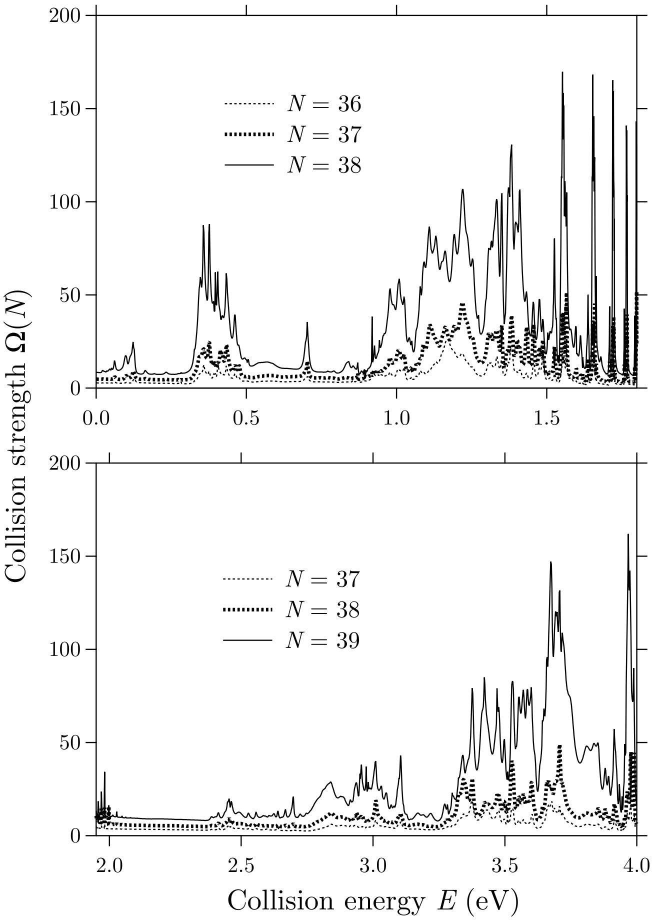

FIG. 8. The final-state selected capture collision strengths $\Omega(N)$ as a function of the collision energy E for the principal quantum numbers $N = 36, 37$, and 38 at $0 \leqslant E \leqslant 1.8$ eV, and for $N = 37, 38$, and 39 at $1.95 \leqslant E \leqslant 4$ eV.

Figure 11 shows the energy dependence of the capture collision strengths $\Omega(L)$ for the formation of $\bar{p}\mathrm{He}^{2+}(L)$ with angular momentum $L = 5, 15, 25$, and 35. The details of the L distribution $\Omega(L)/\Omega$ of the products $\bar{p}\mathrm{He}^{2+}$ are shown in Fig. 12 at three collision energies. In contrast to the N distribution, the resonances make the pattern of the L distribution quite different according to the energy, and furthermore any (even very low or very high) state in the range $0 \leqslant L \leqslant 38$ can have a finite population. It seems that very high L states are produced effectively rather through high Rydberg resonances. In the energy region where no prominent resonance occurs ($E = 2.3$ eV in Fig. 12), the L distribution forms roughly a smooth curve and reflects the statistical weight $\propto (2L + 1)$ for the angular momenta up to $L \simeq 20$ for which $\Omega(L)/\Omega$ becomes the maximum. In Fig. 10, we can see that the average angular momentum $\langle L \rangle$ gives values fluctuating sharply around ~20, and the range of fluctuation is much wider than that of $\langle N \rangle$ owing to the resonances.

D. Energy-averaged capture cross section

Let us take another look at the capture cross sections with finite resolution of collision energies. We average the cross sections over the energy interval $(E - \Delta E/2, E + \Delta E/2)$,

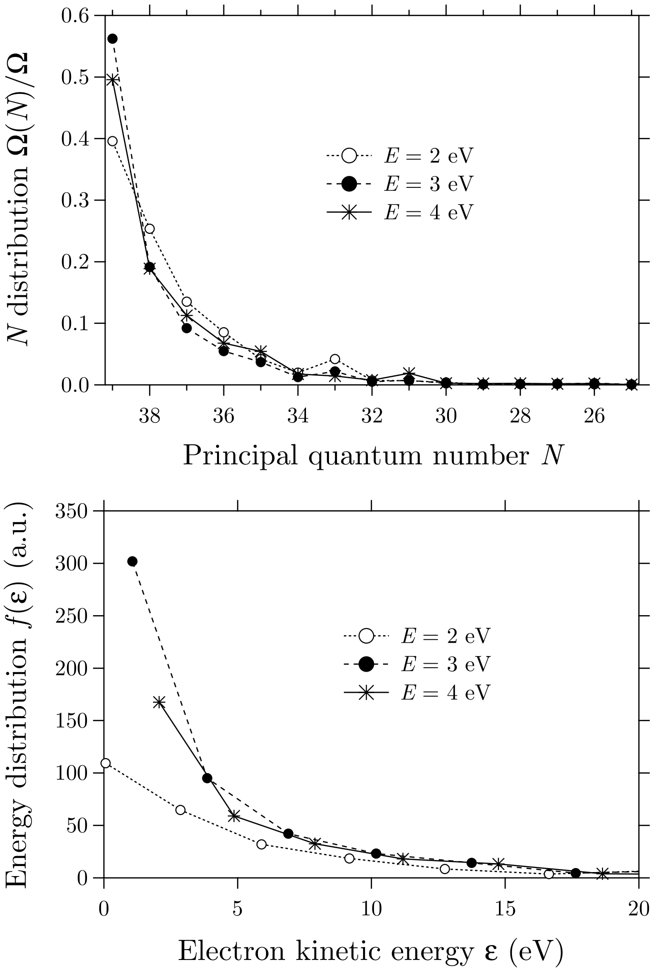

FIG. 9. The N distributions $\Omega(N)/\Omega$ of the products $\bar{p}\mathrm{He}^{2+}$ (upper panel) and the kinetic energy distributions $f(\varepsilon)$ of the emitted electrons (lower panel). The collision energies are $E = 2$, 3, and 4 eV.

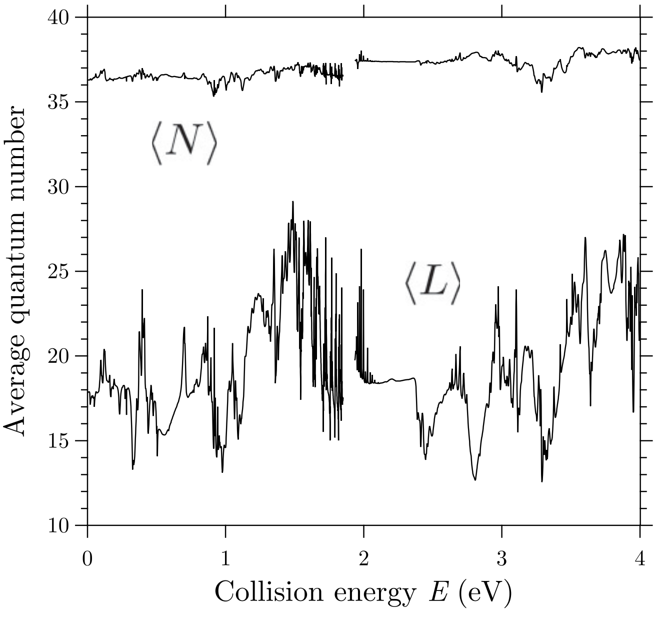

FIG. 10. Average quantum numbers $\langle N \rangle = \sum_N N\,\Omega(N)/\Omega$ and $\langle L \rangle = \sum_L L\,\Omega(L)/\Omega$ at collision energies $0 \leqslant E \leqslant 4$ eV.

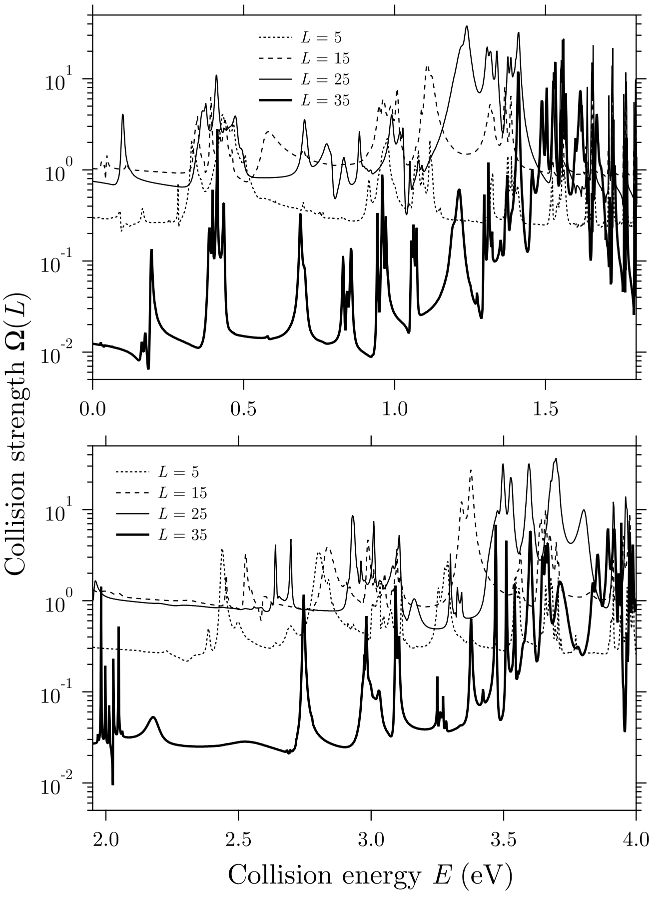

FIG. 11. The final-state selected capture collision strengths $\Omega(L)$ as a function of the collision energy E for the angular momenta $L = 5$, 15, 25, and 35 at $0 \leqslant E \leqslant 1.8$ eV and at $1.95 \leqslant E \leqslant 4$ eV.

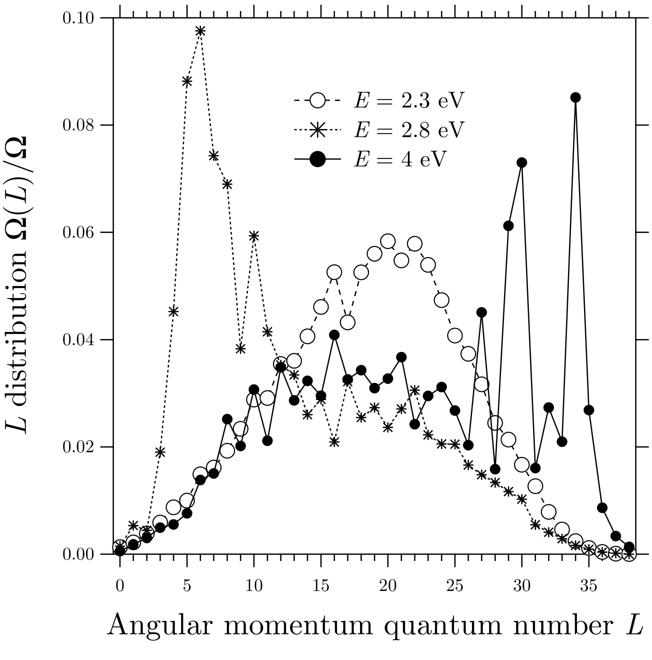

FIG. 12. The L distributions $\Omega(L)/\Omega$ of the products $\bar{p}\mathrm{He}^{2+}$ at collision energies $E = 2.3$, 2.8, and 4 eV.

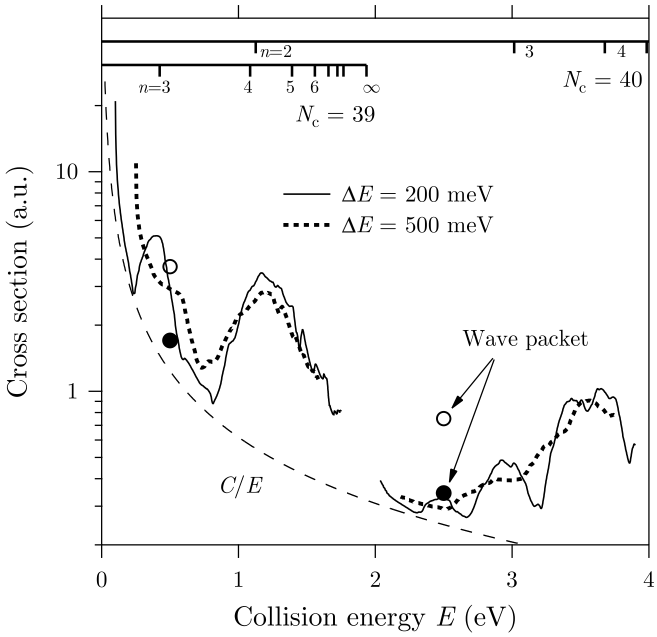

FIG. 13. The energy-averaged capture cross sections, $\langle\sigma\rangle$, summed over all the final product channels at collision energies $0 < E < 4$ eV. The energy resolutions are $\Delta E = 200$ and 500 meV. Also plotted are the cross sections obtained by Eq. (24) and the cross sections for the direct capture (●) and for the direct plus resonance capture (○) obtained in Ref. [9] using the wave packet propagation method. The hydrogenic levels $E^{\mathrm{H}}_{N_c,n} - D$ for $N_c = 39$ and 40 are denoted by vertical bars on the top of the figure.

where ΔE may correspond to the experimental energy resolution:

$$\langle\sigma\rangle = \frac{1}{\Delta E}\int_{E-\frac{1}{2}\Delta E}^{E+\frac{1}{2}\Delta E} \sigma \, dE. \tag{25}$$

Figure 13 shows the energy-averaged capture cross sections summed over all the final product channels for the resolutions $\Delta E = 200$ and 500 meV. With the energy resolution $\Delta E = 200$ meV, the resonances identified as $n = 3$ are smoothed to form a single peak structure, and the $n = 4$ and 5 resonances all together seem to appear as a broad peak. No further notable peak structure can be seen for the $n \gtrsim 6$ resonances. With $\Delta E = 500$ meV, the $n = 3$ peak becomes obscure although the $n = 4$ and 5 broad peak remains. We also plot the cross section obtained by Eq. (24), which is expected to give the background (direct) contribution of the capture cross section at low energies. It is evident that the averaged cross sections are significantly enhanced from the background values in the resonance region.

The present author calculated the capture cross sections in $\bar{p} + \mathrm{He}^+$ by using the time-dependent wave packet propagation method [9]. However, the detailed structure of the resonances could not be resolved, and the results were presented separately for the direct cross sections and for the resonance part of the cross sections averaged over the resonances. Figure 13 also includes these results. (Here, the central energy of the wave packet [9], which has a certain energy distribution, serves as a substitute for the collision energy.) The direct cross sections of Ref. [9] are close to the present background values. In Ref. [9], the direct cross section at $E = 0.5$ eV was fitted to the form of Eq. (24) to provide $C_{\mathrm{WP}} = 0.844$, which is 40% larger than the present value of the low-energy limit. The total (direct plus resonance) cross section of Ref. [9] is also close to the present energy-averaged result at $E = 0.5$ eV, but it is much larger than the present result at $E = 2.5$ eV. Probably, the reason for the latter is that the wave packet used in Ref. [9], which has the distribution over a wide energy range $0 \leqslant E \lesssim 6$ eV, inevitably includes a huge number of irrelevant resonances, while no prominent resonances can be observed around $E = 2.5$ eV in the present calculation. Cohen calculated the capture cross sections in $\bar{p} + \mathrm{He}^+$ by using a fermion-molecular-dynamics method, in which the classical-trajectory analysis is employed with some quantum corrections [37]. However, his results are far too much larger than the present values and are not shown here.

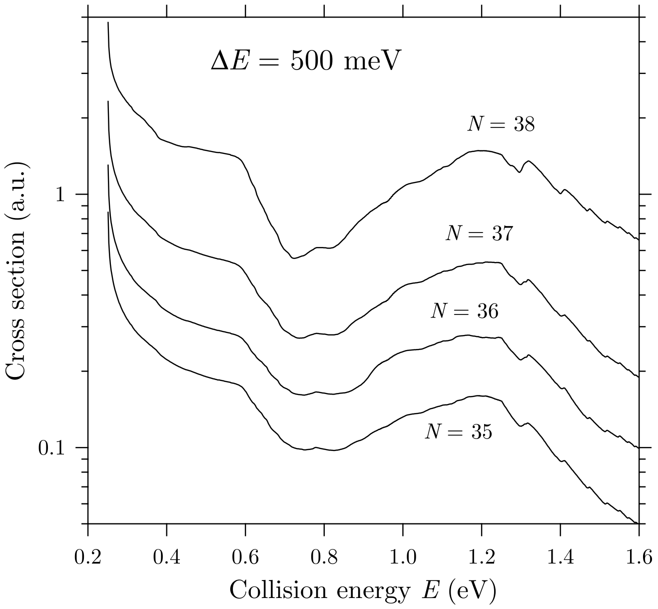

FIG. 14. The energy-averaged capture cross sections for the formation of $\bar{p}\mathrm{He}^{2+}(N)$ with $N = 35$–38 at collision energies $0.2 < E \leqslant 1.6$ eV. The energy resolution is $\Delta E = 500$ meV.

For the capture into $\bar{p}\mathrm{He}^{2+}(N)$ with N specified, the energy-averaged cross sections calculated with the resolution $\Delta E = 500$ meV are presented for $N = 35$–38 at collision energies $E \leqslant 1.6$ eV in Fig. 14. The averaged cross sections for all these N have a similar shape, although the magnitude varies significantly.

E. Capture rate coefficient

Finally, we calculate the capture rate coefficients thermally averaged over collision energies, which are given by

$$k = \frac{(2\pi)^{1/2}}{(\mu\kappa T)^{3/2}}\int_0^\infty \Omega \exp(-E/\kappa T)\, dE, \tag{26}$$

where κ is the Boltzmann constant and T is the temperature. The rate coefficients summed over all the final product channels are shown in Fig. 15 in the temperature range $1 \leqslant T \leqslant 10\,000$ K. We also plot the rate coefficients $k_0 = (2\pi/kT)^{1/2} m^{-3/2}\Omega$ obtained by assuming that the collision

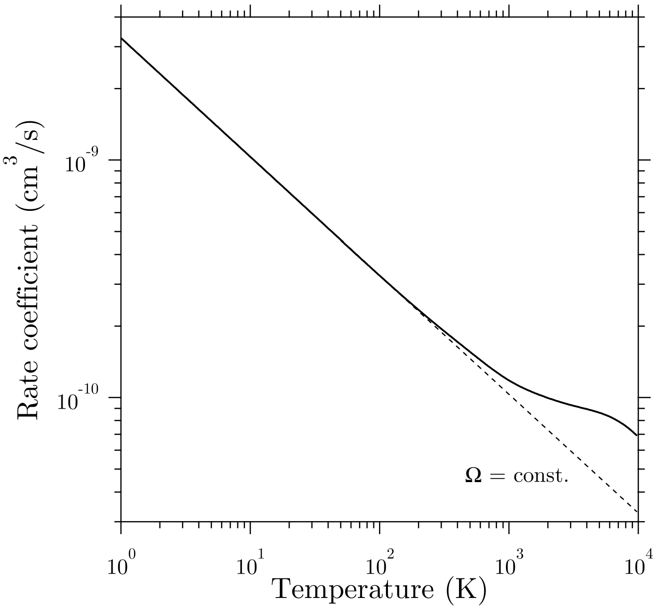

FIG. 15. The capture rate coefficients k summed over all the final product channels at temperatures $1 \leqslant T \leqslant 10\,000$ K. Also shown are the rate coefficients k_0 obtained by assuming that Ω (=21.2) is independent of E.

strength is constant ($\Omega = 21.2$) as in Eq. (24). If the values of k_0 can be regarded as the contribution of the direct capture, we can see that the resonances become important at temperatures $T > 1000$ K.

For the capture into $\bar{p}\text{He}^{2+}(N)$ or $\bar{p}\text{He}^{2+}(L)$, the rate coefficients are plotted in Fig. 16. The rate coefficient becomes the maximum for the formation of $\bar{p}\text{He}^{2+}$ having $N = 38$ and $L \sim 20$ at low temperatures. At $T \leqslant 1000$ K, the state distributions have a similar shape except for the magnitude. In the case that the resonances are expected to be important ($T = 10\,000$ K), however, the state distribution seems to be somewhat different from the ones at other temperatures.

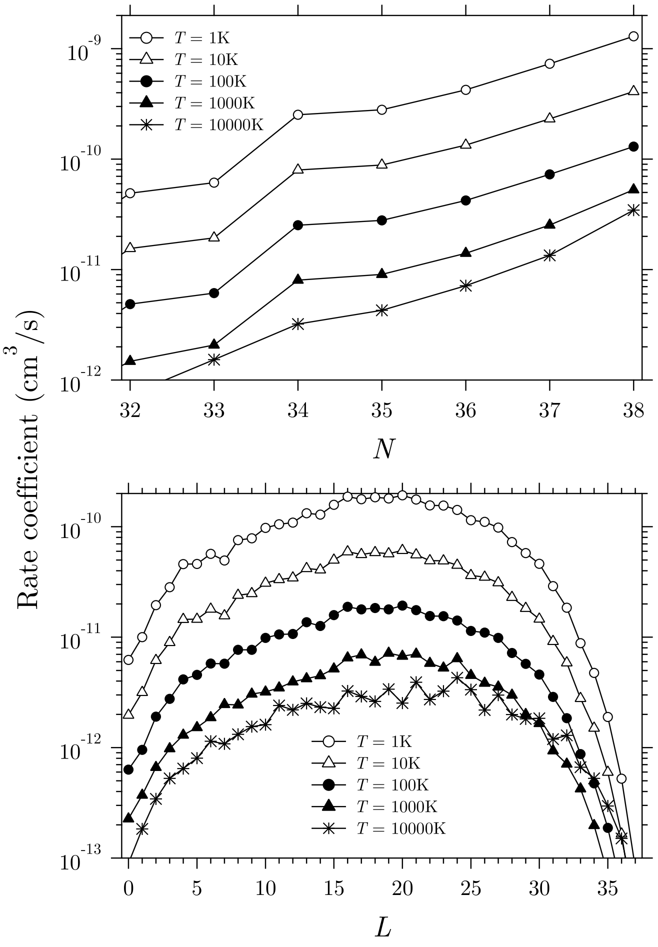

FIG. 16. The capture rate coefficients for the formation of $\bar{p}\text{He}^{2+}(N)$ and of $\bar{p}\text{He}^{2+}(L)$ at temperatures T = 1, 10, 100, 1000, and 10 000 K.

IV. FURTHER DISCUSSION

The low angular momentum states of $\bar{p}\text{He}^{2+}$ are unstable because they decay via pair annihilation [3,30]. If their lifetime against the annihilation were shorter than the collision time of the capture reaction, these states could not be observed as the $\bar{p}\text{He}^{2+}$ products. The annihilation widths of the (N,L) state can be given by

$$\Gamma_{NS} = \frac{1}{N^3}\Gamma_{1S}, \tag{27}$$

$$\Gamma_{NP} = \frac{32}{3}\left(\frac{1}{N^3} - \frac{3}{N^5}\right)\Gamma_{2P}, \tag{28}$$

$$\Gamma_{ND} = \frac{2187}{40}\left(\frac{1}{N^3} - \frac{5}{N^5} + \frac{4}{N^7}\right)\Gamma_{3D}, \tag{29}$$

$$\Gamma_{NF} = \frac{65536}{315}\left(\frac{1}{N^3} - \frac{14}{N^5} + \frac{49}{N^7} - \frac{36}{N^9}\right)\Gamma_{4F}, \tag{30}$$

with $\Gamma_{1S} = 11.1$ keV, $\Gamma_{2P} = 35$ eV, $\Gamma_{3D} = 2.07$ meV, and $\Gamma_{4F} = 0.014$ μeV [30]. If we consider $N = 38$, which is the highest and most populated state of $\bar{p}\text{He}^{2+}$ in the low-energy capture, the annihilation lifetimes can be estimated to be $\tau_{38S} \simeq 3 \times 10^{-15}$ s, $\tau_{38P} \simeq 10^{-13}$ s, $\tau_{38D} \simeq 3 \times 10^{-10}$ s, and $\tau_{38F} \simeq 10^{-5}$ s. The typical collision time τ_{coll} at very low energies may be defined by the passage time from $R = A$ to $R = 0$ ($J = 0$) under the Coulomb force $-1/R$. At $E = 0$, this gives $\tau_{\text{coll}} = 6.5 \times 10^{-16}$ s, which is much shorter than the annihilation lifetimes for $L \geqslant 1$. Therefore, the capture into $\bar{p}\text{He}^{2+}$ having $N = 38$ and $L \geqslant 1$ at low energies can be counted as an atomic event without any problem. Although the resonance phenomenon makes the collision time much longer, the annihilation in the resonance capture process would be significant at most only for $L = 0$ and 1 unless n is extremely large. It should be noted that if the detection of $\bar{p}\text{He}^{2+}$ needs a long time (of $\gg$ microseconds) in means of measurement, the annihilation of the L = 0–3 states may be one of the loss processes of $\bar{p}\text{He}^{2+}$ in an experimental study. In any case, the annihilation effect is negligible for the determination of the actual value of the total capture cross section, to which a lot of angular momentum states up to $L \gtrsim 35$ always contribute. After the capture reaction is completed, the annihilation of the resultant $\bar{p}\text{He}^{2+}$, even if having initially high L, will be further activated by the L mixing, which is induced by collisions with other particles (or

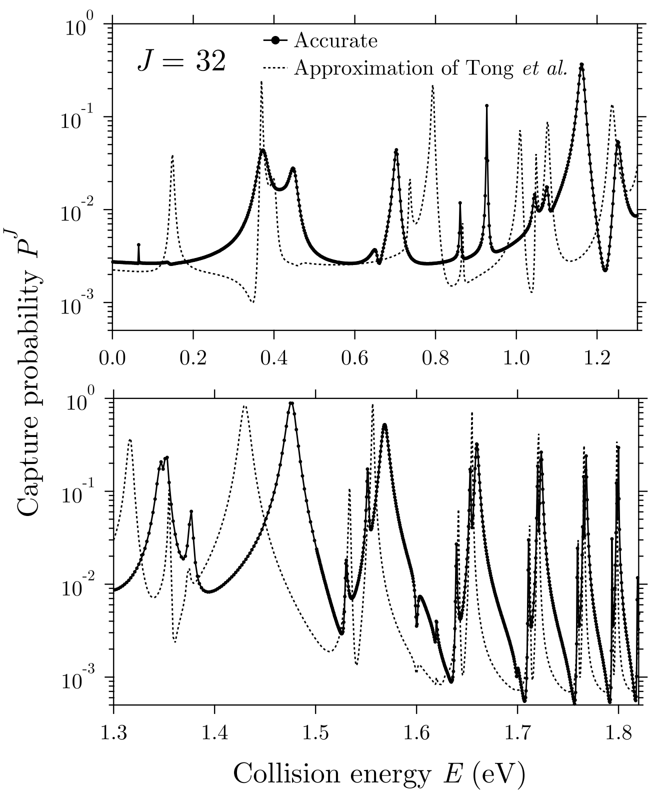

FIG. 17. The total capture probabilities P^J for the total angular momentum $J = 32$ at collision energies $0 \leqslant E \leqslant 1.82$ eV obtained by using the accurate method and the approximation of Tong *et al.* [21].

possibly by external fields) [38–42]. The L-mixing processes are very important for understanding the atomic cascade and the lifetime history of $\bar{p}\text{He}^{2+}$ [3,30,31,38,39].

In the calculation of the $\bar{p}$ capture by He, Tong *et al.* [21] introduced the approximation, in which the coordinate origin was set to He^{2+} and the resulting cross term in the kinetic energy operators was neglected. As mentioned in Sec. I, this approximation makes the numerical calculation much more tractable. Since the present system has the same mass combination as that of $\bar{p} + \text{He}$ except for the additional electron, it is interesting to examine to what extent this approximation is appropriate for the present capture process. In Fig. 17, we compare the total capture probabilities of $\bar{p} + \text{He}^+$ for $J = 32$ calculated by using this approximation with the present accurate results. The approximation of Tong *et al.* may not be so bad for the high Rydberg resonance capture and possibly for the direct capture, but it no longer serves a useful purpose for other prominent resonances. Although the resonance capture is absolutely not important for the neutral He target, we should note that the present result raises questions about the use of the approximation of Tong *et al.* in the $\bar{p} + \text{He}$ system. Furthermore, the description of the state distribution should be sensitive to the choice of the coordinate system. The approximation of Tong *et al.* would be a little more useful for the targets much heavier than the He atom. If this approximation is poor for the $\bar{p} + \text{He}$ system, it is so much the worse for the $\bar{p} + \text{H}$ system because $m_{\bar{p}} = m_p < m_\alpha$. However, Tong *et al.* introduced this approximation to analyze the final-state distributions in the $\bar{p}$ capture by H [19,20]. The coordinate problem is obstructive to the accurate numerical treatment in this system. It is highly desirable to progress a theoretical study on the subject of the $\bar{p}$ capture by H.

ACKNOWLEDGMENTS

The present work was partially supported by the Grant-in-Aid for Scientific Research (C) from the Japan Society for the Promotion of Science.

---

[1] C. J. Batty, Rep. Prog. Phys. **52**, 1165 (1989).
[2] E. Klempt, F. Bradamante, A. Martin, and J. M. Richard, Phys. Rep. **368**, 119 (2002).
[3] D. Gotta, Prog. Part. Nucl. Phys. **52**, 133 (2004).
[4] E. Fermi and E. Teller, Phys. Rev. **72**, 399 (1947).
[5] A. S. Wightman, Phys. Rev. **77**, 521 (1950).
[6] J. S. Cohen, Rep. Prog. Phys. **67**, 1769 (2004).
[7] R. Ahlrichs, O. Dumbrajs, H. Pilkuhn, and H. G. Schlaile, Z. Phys. A **306**, 297 (1982).
[8] I. Shimamura, Phys. Rev. A **46**, 3776 (1992).
[9] K. Sakimoto, Phys. Rev. A **74**, 022709 (2006).
[10] K. Sakimoto, Phys. Rev. A **79**, 042508 (2009).
[11] T. Yamazaki, N. Morita, R. S. Hayano, E. Widmann, and J. Eades, Phys. Rep. **366**, 183 (2002).
[12] R. S. Hayano, M. Hori, D. Horváth, and E. Widmann, Rep. Prog. Phys. **70**, 1995 (2007).
[13] N. Elander and E. Yarevsky, Phys. Rev. A **56**, 1855 (1997).
[14] V. I. Korobov and I. Shimamura, Phys. Rev. A **56**, 4587 (1997).
[15] J. Révai and A. T. Kruppa, Phys. Rev. A **57**, 174 (1998).
[16] O. I. Kartavtsev, D. E. Monakhov, and S. I. Fedotov, Phys. Rev. A **61**, 062507 (2000).
[17] Y. Kino, M. Kamimura, and H. Kudo, Nucl. Instrum. Methods Phys. Res. B **214**, 84 (2004).
[18] K. Sakimoto, Phys. Rev. A **65**, 012706 (2001).
[19] X. M. Tong, K. Hino, and N. Toshima, Phys. Rev. Lett. **97**, 243202 (2006).
[20] X. M. Tong, T. Shirahama, K. Hino, and N. Toshima, Phys. Rev. A **75**, 052711 (2007).
[21] X. M. Tong, K. Hino, and N. Toshima, Phys. Rev. Lett. **101**, 163201 (2008).
[22] A. K. Bhatia and A. Temkin, Phys. Rev. **137**, A1335 (1965).
[23] B. D. Esry and H. R. Sadeghpour, Phys. Rev. A **67**, 012704 (2003).
[24] M. Hesse, A. T. Le, and C. D. Lin, Phys. Rev. A **69**, 052712 (2004).
[25] K. Sakimoto, Phys. Rev. A **80**, 012517 (2009).
[26] K. Sakimoto, Phys. Rev. A **78**, 042509 (2008).
[27] K. Sakimoto, Phys. Rev. A **81**, 012511 (2010).
[28] P. G. Burke and W. D. Robb, Adv. At. Mol. Phys. **11**, 143 (1975).
[29] K. Sakimoto, Phys. Rev. A **76**, 042513 (2007). In the calculation of this reference, the phase choice of the associated Legendre

functions was not consistent with the conventional definition of the Clebsch-Gordan coefficients. As a result, some resonance profiles were wrong. For the details of the resonances, see Ref. [10] or the present paper.

[30] C. A. Baker *et al.*, Nucl. Phys. A **494**, 507 (1989).

[31] M. Hori *et al.*, Phys. Rev. Lett. **94**, 063401 (2005).

[32] C. Bloch, Nucl. Phys. **4**, 503 (1957).

[33] M. J. Seaton, Rep. Prog. Phys. **46**, 167 (1983).

[34] C. H. Greene and Ch. Jungen, Adv. At. Mol. Phys. **21**, 51 (1985).

[35] M. Gailitis, Sov. Phys. JETP **17**, 1328 (1963).

[36] K. Sakimoto, Phys. Rev. A **66**, 032506 (2002).

[37] J. S. Cohen, Phys. Rev. A **69**, 022501 (2004).

[38] T. B. Day, G. A. Snow, and J. Sucher, Phys. Rev. Lett. **3**, 61 (1959).

[39] M. Leon and H. A. Behte, Phys. Rev. **127**, 636 (1962).

[40] T. S. Jensen and V. E. Markushin, Eur. Phys. J. D **19**, 165 (2002).

[41] K. Sakimoto, J. Phys. B **38**, 3447 (2005).

[42] A. Igarashi and L. Gulyás, J. Phys. B **42**, 035201 (2009).